2012-02

Optical properties of amorphous, erbium-doped yttrium alumino-borate thin films

Optical Materials,Amsterdam : Elsevier BV,v. 34, n. 4, p. 665-670, Feb. 2012
http://www.producao.usp.br/handle/BDPI/49770

Optical Materials 34 (2012) 665–670

Contents lists available at SciVerse ScienceDirect

Optical Materials

journal homepage: www.elsevier.com/locate/optmat

Optical properties of amorphous, erbium-doped yttrium alumino-borate thin films

L.J.Q. Maia [a,*], J. Fick [b], A.C. Hernandes [c], V.R. Mastelaro [c], A. Ibanez [b]

[a] Grupo Física de Materiais, IF – Universidade Federal de Goiás, Caixa Postal 131, 74001-970 Goiânia, GO, Brazil
[b] Institut Néel, CNRS & Université Joseph Fourier, 25 Avenue des Martyrs, BP 166, 38042 Grenoble, France
[c] Grupo Crescimento de Cristais e Materiais Cerâmicos, IFSC – Universidade de São Paulo, Caixa Postal 369, 13560-970 São Carlos, SP, Brazil

ARTICLE INFO

Article history:
Received 20 June 2011
Received in revised form 21 September 2011
Accepted 23 September 2011
Available online 13 November 2011

Keywords:
Borate thin films
$Y_{1-x}Er_xAl_3(BO_3)_4$
Soft chemical methods
Waveguides
Photoluminescence
m-Lines spectroscopy

ABSTRACT

In this paper, we report on the optical characterizations of erbium-doped yttrium alumino-borate glassy thin films prepared by the polymeric precursor and sol–gel routes and the spin-coating technique. High quality planar waveguides were produced by a multilayer processing of $Y_{1-x}Er_xAl_3(BO_3)_4$ compositions with $x = 0.02$, 0.05, 0.10, 0.30, and 0.50. Their optical properties were investigated using transmission, photoluminescence, and *m*-lines spectroscopy, whereas high resolution scanning electron microscopy (HR-SEM) was applied to check film thickness and surface homogeneity. The refractive indices determined from transmission and *m*-lines spectroscopy are in good agreement just like the film thickness measured by HR-SEM and transmission spectroscopy. We observed low propagation losses, together with efficient photoluminescence emission for polymeric precursor thin films, involving low cost and environment friendly reactants.

1. Introduction

Currently, considerable attention is devoted to the development of efficient and compact optical waveguide amplifiers and lasers based on rare earth-doped glasses for applications in integrated optical devices [1–4]. Among the rare earth elements, erbium is of potential interest for telecommunications due to its photoluminescence (PL) emission at 1540 nm [5,6]. To achieve high-gain optical amplification in a few centimeter long waveguide, a high erbium concentration is required. Many results have been reported on the spectroscopic properties of erbium-doped matrices, such as silicate, aluminate, phosphate or chalcogenide glasses [7–13]. In silicate matrices the available gain is limited by the onset of concentration quenching at low doping levels. In general, phosphate glasses allow reaching the highest erbium concentrations and appearing as potential host matrices for waveguide optical amplifiers. It is, however, worthwhile to develop other host matrices exhibiting high solubility for rare earth elements to further increase the erbium doping concentration [14].

On the other hand, for bulk crystals, one potential host is yttrium aluminum borate (c-YAB). Indeed, c-YAB exhibits good properties for solid-state lasers: the high physical and chemical stabilities are combined with a high thermal conductivity and good mechanical strength [6,15–18]. In addition, the c-YAB high refractive index ($n = 1.63$) in respect to standard silicate substrates allows to realize high contrast waveguides with good light confinement and thus, higher pumping and amplification efficiencies [19]. In this paper, we report on planar waveguides of doped YAB composition which we denominate a-YAB (a: amorphous) [20–23]. To the best of our knowledge, we are the only group working on this kind of glassy borate thin films.

In a previous paper, we have demonstrated that, similar to other borate glass systems, a-YAB:Er thin films shows high PL emission with lifetimes ranging between 640 and 200 μs [24]. In the present paper, we report the detailed optical characterizations of the a-YAB:Er thin films. The measured parameters include refractive indexes, film thicknesses, optical losses, and PL emissions. High resolution scanning electron microscopy (HR-SEM), Ultraviolet (UV) – Visible – Near Infrared (NIR) transmission spectra, *m*-lines spectroscopy and transmission PL emission spectra collected through the waveguiding geometry were analyzed for different erbium concentrations.

2. Experimental

2.1. Film preparation

To prepare planar waveguides, two chemical routes were selected: the polymeric precursor (PP) and the sol–gel (SG) methods. The main advantages of these soft-chemical processes are the high control of chemical homogeneity and purity of the resulting deposits, the low temperature of synthesis, the easy incorporation of rare earth ions and the possibility to cover large substrate areas

* Corresponding author. Tel.: +55 62 35211122x206; fax: +55 62 35211014.
E-mail address: lauro@if.ufg.br (L.J.Q. Maia).

0925-3467/$ - see front matter © 2011 Elsevier B.V. All rights reserved.
doi:10.1016/j.optmat.2011.09.014

by dip-coating or spin-coating techniques [20,21]. Likewise, they are suitable for the preparation of multi-component systems since different components can be easily mixed in the initial solutions at the molecular level. The main differences between PP and SG methods are the nature of the precursors and the involved polymerization reactions. In the PP syntheses, citric acid and *d*-sorbitol are used as complexing and polymerizing agents, respectively, while carbonates and salts are commonly used for cations precursors [20]. On the other hand, in the sol–gel process, alkoxides and salts are typically involved as precursors while hydrolysis of the former must be carefully controlled [24].

The active materials selected for our experiments are $Y_{1-x}Er_xAl_3(BO_3)_4$ compositions, with $x = 0.02$, 0.05, 0.10, 0.30, and 0.50. For the PP method, Aluminum nitrate nonahydrate (Prolabo 98% purity), boric acid (Carlo Erba 99.8% purity), yttrium nitrate hexahydrate (Aldrich 99.9% purity), and erbium nitrate pentahydrate (Aldrich 99.9% purity) were used as precursors. Citric acid monohydrate (Aldrich 99.5% purity) and *d*-sorbitol (Aldrich 99.5% purity) were used as complexing and polymerizing agents, respectively. The molar ratio of citric acid referred to the constituting elements of the films (metals + boron) was 3:1, while the citric acid/*d*-sorbitol mass ratio was set to 3:2. By heating continuously under stirring at 120 °C, the polymerization occurred through the polyesterification reactions between metallic citrates and boron complexed by *d*-sorbitol forming a polymeric resin as detailed elsewhere [22]. In order to control the film thickness the resin viscosity was adjusted to 25 mPa s by evaporation or by the addition of water.

On the other hand, for the SG method, aluminum acetylacetonate (Aldrich 99% purity), tri-i-propylborate (Strem 98% purity), yttrium nitrate hexahydrate (Aldrich 99.9% purity) and erbium nitrate pentahydrate (Aldrich 99.9% purity) were used as precursors dissolved in ethyl alcohol (EtOH, Riedel-de Haen 99.8% purity) and propionic acid (PropAc, Merck 99% purity). These sol preparations were carried out in a dry glove box (N_2 atmosphere). The hydrolysis of precursors, particularly tri-i-propylborate, was performed at 80 °C/1 h. The molar relatives proportions of YAB constitutive elements (metals + boron):EtOH:PropAc:H_2O were 1:95:55:5 as detailed in Ref. [21]. The resulting sols were filtered at room temperature (26 °C) by using filters of 0.2 μm porosity. During these heat treatments, the solutions were placed into closed silica glass flasks with polypropylene covers. Finally, by removing the covers, the solvents were partially evaporated, around 65 vol.%, at 80 °C during 70 min.

The as-prepared PP resins and SG sols were deposited on silica glass substrates by using a RC8 SussMicrotech™ spin-coater involving the "gyrset" technology to improve film thickness uniformity. Rotation acceleration, rotation speed and spin time were fixed at 500 rpm/s, 2500 rpm, and 5 s, respectively. After the deposition of one layer, the film was dried at 80 °C for 30 min, followed by two intermediary annealing treatments under O_2 atmosphere: one at 400 °C during 2 h with a heating rate of 1 °C/min and a second at 700 °C during 2 h involving a 2 °C/min heating-rate. This thermal procedure was repeated for each layer, nine layers for PP films and seven layers for the SG ones. Finally, the multilayer deposits were annealed at 740 °C for PP and 780 °C for SG during 2 h with a heating rate of 1 °C/min. Additional preparation details are given in Refs. [20,24].

2.2. Measurements

The thickness and chemical homogeneity of the films were characterized by HR-SEM (FEG-VP Supra 35, Zeiss). The optical transmission in the 250–900 nm range was recorded at room temperature using a Perkin–Elmer Lambda 900 spectrophotometer.

The film refractive indexes were measured with an *m*-lines apparatus (Metricon Model 2010) based on prism coupling and using transverse electric (TE) and magnetic (TM) polarizations. A gadolinium garnet (GGG) prism with a refractive index of 1.9644 at 633 nm was used and the angular resolution was 0.0075°. This apparatus is equipped with Si and Ge detectors for visible and NIR wavelengths. Two He–Ne lasers, operating at 543 and 633 nm, and a diode laser, operating at 1538 nm, were employed. The *m*-lines apparatus was also used for loss measurements which were recorded by scanning an optical fiber probe along the propagating light streak. The attenuation coefficient was obtained by fitting the data to an exponential decay function, assuming that the longitudinal scattering center distribution is homogenous with a constant waveguide loss. The loss measurements of the fundamental TE mode were performed at 633 nm on SG and PP films, 5.5 mm and 4.3 mm long, respectively.

The photoluminescence emission spectra were measured at room temperature in the waveguiding configuration on about 3 mm long samples. To obtain good light in- and out-coupling, around 80% of the substrate thickness was sliced with a diamond-steel wire saw on the opposite face to the film. Subsequent cleaving of the substrates results in high quality end-faces. A pigtailed laser diode (Newport 740) emitting at 980 nm (100 mW) was used as excitation source. An optical spectrum analyzer (Hewlet Packard 700004) allowed to record the NIR PL emission spectra, collected at the end of the waveguide by a multimode optical fiber.

3. Results

3.1. Scanning electron microscopy

The HR-SEM micrographs of PP and SG films with $x = 0.10$ are displayed in Fig. 1. The glassy thin films are very homogenous and do not exhibit any porosity. They exhibit well defined air–film and film–substrate interfaces with uniform layer thicknesses. Film thicknesses measured on these HR-SEM images are around 600 nm for the PP method and 516 nm for the SG one. For films with different compositions, the deposition conditions were identical, suggesting similar thicknesses and high quality interfaces.

3.2. Optical transmission

Fig. 2 displays typical transmission spectra for PP and SG films illustrated here for the composition $x = 0.05$. All the films exhibit good transparency, higher than 85%, with clear interference fringes. We applied the envelope method [25,26] to deduce film thicknesses and refractive indices from the fringes distance and contrast. The good agreement between fitted and experimental curves confirms the high homogeneity of the films and the low roughness of air–film and film–substrate interfaces (Fig. 2) as previously observed by HR-SEM. In Fig. 3a and b are presented the calculated refractive index, n, as a function of wavelength, λ, for all PP and SG thin films.

These refractive index evolutions are similar to those reported for the $Y_{0.94}Er_{0.06}Al_3(BO_3)_4$ single crystal. From 900 to 400 nm the film index variations are low, while strong changes occurs between 400 and 250 nm due to the optical band gap proximity, shorter than 190 nm [27]. It should be noted that the refractive index values of the films at 633 nm are slightly lower than those reported for Er-doped YAB crystal with $x = 0.06$ ($n_o = 1.7757$ and $n_e = 1.7015$) [28], which is a very consistent result due to the a-YAB glassy structure of these layers. Note that all the refractive indices of SG thin films are higher than those of PP ones. This is related to the glass structure of the films, as discussed below.

The "envelope method" allowed also determining the film thickness, d. The resulting d values are listed in Table 1 as a func-

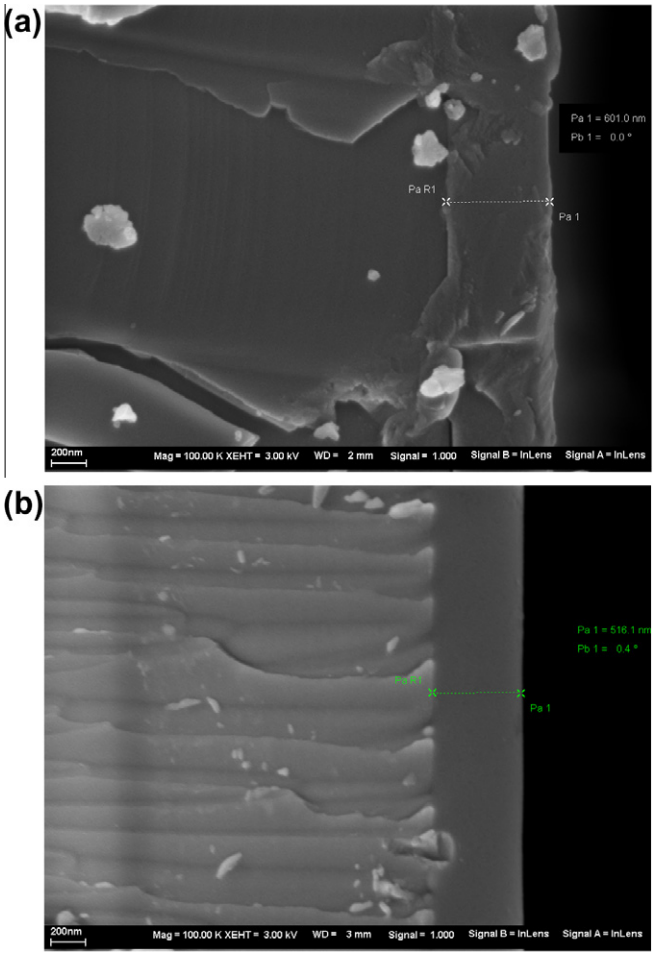

Fig. 1. HR-SEM cross-section micrographs of $x = 0.10$ thin films coated on silicon substrates, annealed at (a) 740 °C for the PP thin film and (b) at 780 °C for the SG deposit.

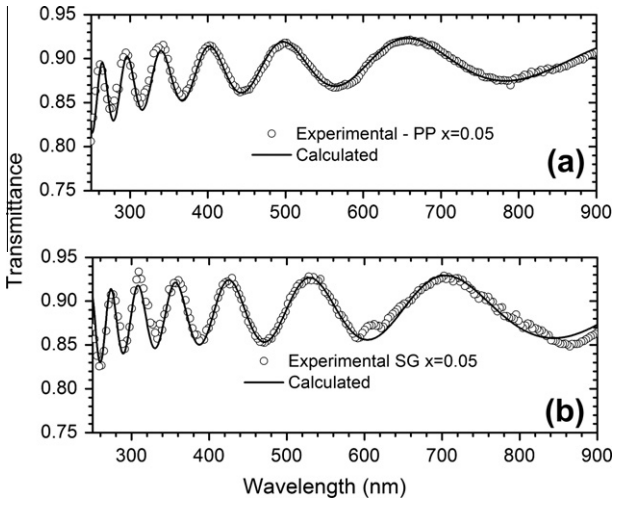

Fig. 2. UV – Visible – NIR optical transmission spectra of $x = 0.05$ films coated on fused silica substrates for PP (a) and SG (b, circles) thin films. The solid lines are the calculated transmission spectra.

tion of the erbium concentration, x, and synthesis methods. The thicknesses for $x = 0.10$ are similar to the HR-SEM measurements, that confirms the validity of the calculated n values.

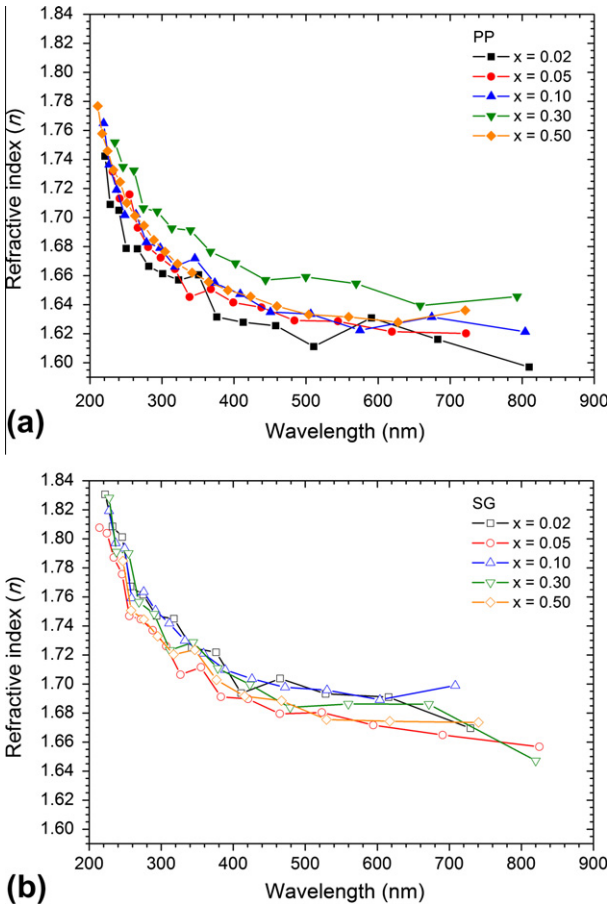

Fig. 3. Refractive index values of $Y_{1-x}Er_xAl_3(BO_3)_4$ thin films as a function of wavelength, deposited on silica substrates for PP(a) and SG(b) thin films, determined by the envelope method (symbols). The solid lines are a guide to the eye.

3.3. m-Lines spectroscopy

The refractive indices and film thicknesses were also calculated from $TE_{0,1}$ and $TM_{0,1}$ lines positions. Fig. 4 shows the refractive indices of PP and SG films in terms of the erbium concentration, at 543 nm, 633 nm, and 1538 nm. Film of almost all compositions support two TE and TM modes at 543 and 633 nm, but only one mode at 1538 nm (Table 1). The thicknesses of the PP and SG films obtained from m-lines results are also shown in Table 1. These values of m-lines refractive indexes are similar to those previously obtained from the optical transmission spectra (Fig. 3). It was observed that the PP films exhibit a minimum for $x = 0.05$, while that of SG films is for $x = 0.10$. This feature reveals again the structural differences between the films prepared by PP and SG. On the other hand, all these layers, exhibiting high refractive index differences with the silica substrate, $\Delta n = n - n_{substrate} \sim 0.18–0.25$, allow to apply good light confinements. Indeed, the thicknesses of these waveguides, in between 500 and 800 nm, are already convenient for single mode propagation of the erbium pump and signal wavelengths at $\lambda = 980$ and 1550 nm, respectively. On the other hand, our glassy thin films have a low birefringence (Fig. 4a and b), except for the PP film with $x = 0.05$ at 633 nm, and for the SG one with $x = 0.10$ at 633 nm and 1538 nm. In fact, almost all the samples have refractive index difference between TE and TM modes (Δ) lower than 0.002. Homogenous films possess birefringence of form due to difference of p- and s-polarized light reflections on film surface. There is also birefringence due to stress between

Table 1
Compilation of the determined values of refractive indices, thicknesses and modes numbers for $Y_{1-x}Er_xAl_3(BO_3)_4$ glassy thin films coated on silica substrates from PP and SG methods at different wavelengths and Er concentrations, *x*.

x	Method	Wavelength (nm)	Refractive index (*n*)		No. of modes	Thickness from *m*-lines (nm)	Thickness from Envelope method (nm)
			Envelope method	*m*-lines			
0.02	PP	543	1.62 ± 0.01	1.6437 ± 0.0005	2	639 ± 12	634 ± 7
		633	1.624 ± 0.008	1.636 ± 0.002	2		
		1538	-	1.621 ± 0.001	1		
	SG	543	1.692 ± 0.002	1.683 ± 0.001	2	496 ± 5	546 ± 7
		633	1.68 ± 0.01	1.6735 ± 0.0002	2		
		1538	-	1.6518 ± 0.0003	1		
0.05	PP	543	1.6288 ± 0.0003	1.637 ± 0.003	2	686 ± 16	669 ± 5
		633	1.6207 ± 0.0006	1.61 ± 0.01	2		
		1538	-	1.610 ± 0.001	1		
	SG	543	1.676 ± 0.004	1.6738 ± 0.0007	2	553 ± 4	622 ± 4
		633	1.668 ± 0.003	1.663 ± 0.001	2		
		1538	-	1.64690 ± 0.00004	1		
0.10	PP	543	1.628 ± 0.006	1.6451 ± 0.0008	2	678 ± 5	620 ± 7
		633	1.627 ± 0.005	1.6359 ± 0.0003	2		
		1538	-	1.6156 ± 0.0004	1		
	SG	543	1.693 ± 0.003	1.666 ± 0.003	2	590 ± 16	625 ± 7
		633	1.694 ± 0.005	1.658 ± 0.004	1		
		1538	-	1.637 ± 0.002	1		
0.30	PP	543	1.657 ± 0.002	1.6477 ± 0.0006	2	609 ± 4	602 ± 4
		633	1.647 ± 0.008	1.6389 ± 0.0006	2		
		1538	-	1.6202 ± 0.0002	1		
	SG	543	1.685 ± 0.001	1.6775 ± 0.0006	2	631 ± 3	498 ± 6
		633	1.6862 ± 0.0001	1.6677 ± 0.0006	2		
		1538	-	1.65030 ± 0.00009	1		
0.50	PP	543	1.6324 ± 0.0009	1.6478 ± 0.0003	2	616 ± 5	771 ± 5
		633	1.632 ± 0.004	1.6391 ± 0.0008	2		
		1538	-	1.6212 ± 0.0004	1		
	SG	543	1.6749 ± 0.0006	1.6784 ± 0.0005	2	639 ± 13	553 ± 6
		633	1.6739 ± 0.0004	1.668 ± 0.002	2		
		1538	-	1.651 ± 0.001	1		

the a-YAB:Er film and silica substrate. In our case, the low birefringence indicates homogenous and well amorphous thin films. It was observed that the $x = 0.10$ films have low propagation losses for the TE_0 mode excited at 633 nm, being 0.70 ± 0.13 dB/cm for the SG thin films and 0.52 ± 0.14 dB/cm for the PP ones. Our waveguides exhibit good attenuation coefficients by comparing with other silica based erbium-doped thin films, such as $90SiO_2$–$10GeO_2$–$20AlO_{1.5}$ (~2.0 dB/cm) [29], or $75SiO_2$–$25GeO_2$ (~0.3 dB/cm at 1550 nm) [30].

Fig. 5 illustrates a comparison between the refractive indices calculated from the envelope method and *m*-lines spectroscopy at 633 nm for PP and SG films as a function of Er concentration, *x*. Note that the incorporation of erbium ions in the a-YAB matrix leads to a reduction of the refractive index for $x = 0.05$ and/or $x = 0.10$ compositions. In the case of PP thin films, similar refractive index results were obtained from *m*-lines and transmission spectra for all compositions, being lower than $x = 0.05$ and higher than $x = 0.20$, while significant discrepancies are observed in the case of SG films for $x = 0.1$ and $x = 0.3$ Er concentrations.

3.4. Photoluminescence Emission

Fig. 6 shows the transmission PL emission spectra of PP and SG films measured in the waveguiding geometry. The broad PL emission is typical for the $^4I_{13/2} \rightarrow {}^4I_{15/2}$ transition of erbium ions inside a glassy matrix. The zero Stark shift emission peak at 1530 nm is clearly distinguishable for all films with exception of the $x = 0.30$ ones and the SG film $x = 0.50$, which emission intensity is low. For both film types the integrated emission intensity shows a clear maximum at $x = 0.10$ [24]. These maxima were related to the quenching concentrations which were measured to be around 3 mol.% ($Er_{1.5}O$) in between $x = 0.1$ and 0.3.

4. Discussion

The optical transmission spectra of all the PP and SG thin films can be well fitted by the envelope method [25,26,28], allowing to determine the refractive indices and film thicknesses (Figs. 3 and 5, Table 1) for comparison with *m*-lines results (Figs. 4 and 5, Table 1). The significant gap of refractive index between PP and SG films can be explained in terms of different structural arrangements and relative amounts of BO_3 and BO_4 basic units. Indeed, in a previous paper [23], we have shown that $Y_{0.9}Er_{0.1}Al_3(BO_3)_4$ glassy compounds prepared from the SG method contain higher BO_4/BO_3 ratios than those obtained from the PP route. This higher BO_4 proportion leads to a more connected glassy network and dense structure in agreement with higher refractive indices of the SG thin films than the PP ones [24].

Moreover, we have observed a refractive index minimum around $x = 0.05$ or 0.10 for all wavelengths by *m*-lines spectroscopy (Table 1 and Fig. 4a). This feature can be explained by the glass structure densification process. Pisarski [31] observed that the glass transition temperatures T_g, the crystallization onset temperature T_x, and their differences $\Delta T = T_g - T_x$ evolve when erbium concentration is increased in PbO–PbF_2–B_2O_3–Al_2O_3–WO_3 oxyfluoride glasses showing a maximum of the ΔT value at around 1 wt.%. Analyzing our refractive index values, which are related to the matrix densities, we suppose a dependence of the matrix densification

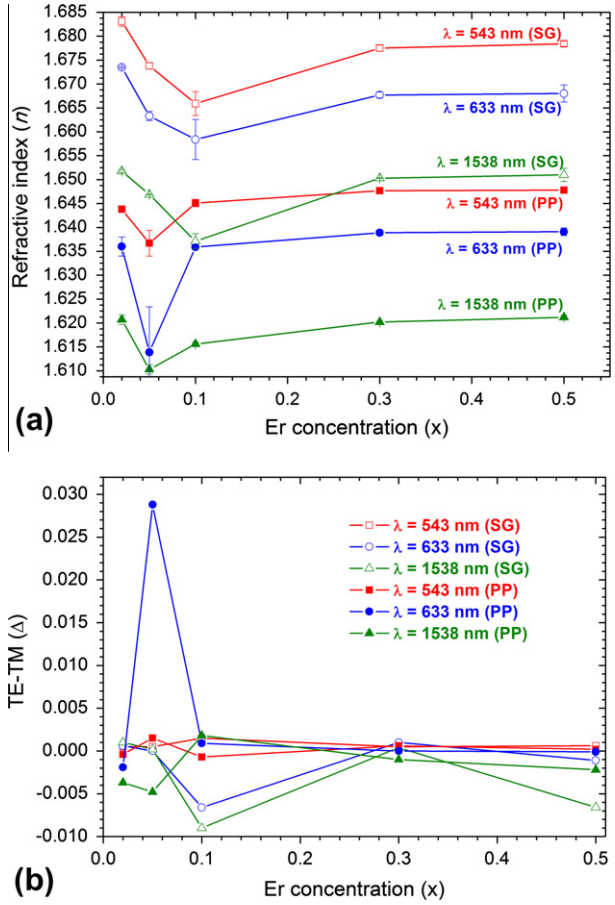

Fig. 4. Refractive index at 543 nm, $\lambda = 633$ nm, and 1538 nm of the PP and SG thin films as a function of Er concentration, calculated from *m*-lines spectroscopy. The solid lines are a guide to the eye.

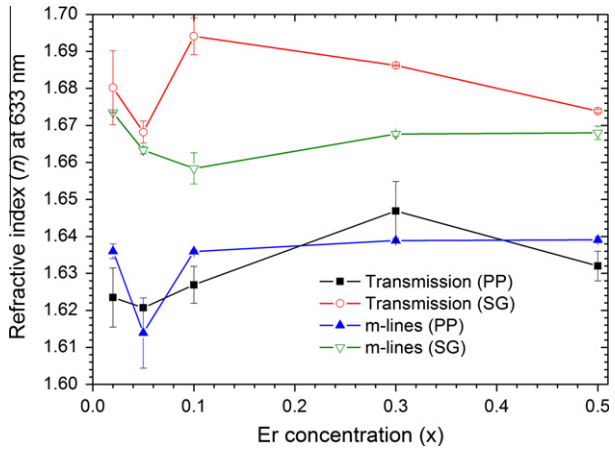

Fig. 5. Comparison between the refractive index at $\lambda = 633$ nm calculated from optical transmission spectra and *m*-lines spectroscopy for PP and SG thin films with different erbium concentrations, *x*. The solid lines are a guide to the eye.

with respect to the annealing temperature for each erbium concentration. As all the films containing different erbium concentrations are annealed at the same temperature (740 °C for PP and 780 °C for SG films [24,32]), this can leads to different matrix densification due to $T_{g(x)}$ evolution. Detailed thermal and structural studies will be required to specify this erbium concentration effect on the refractive index.

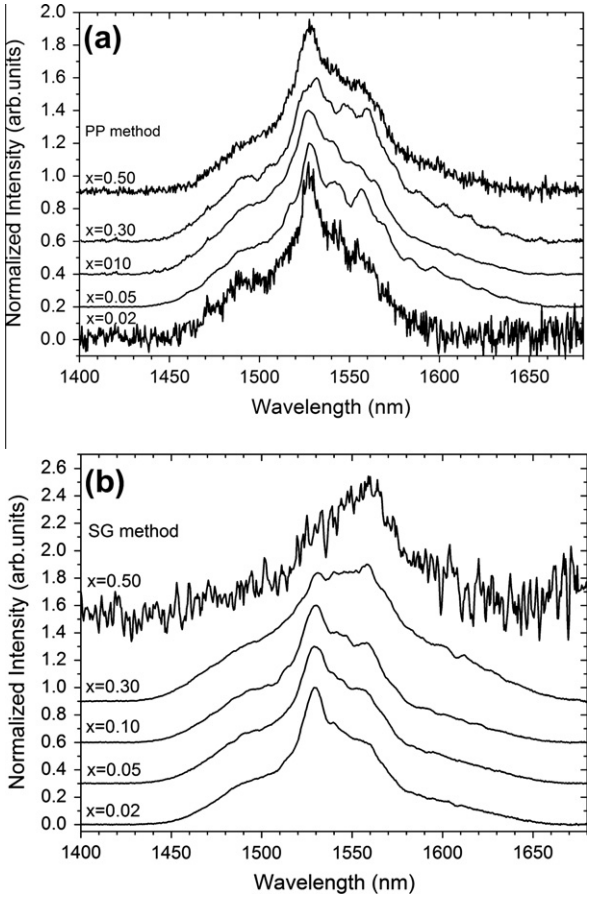

Fig. 6. PL emission spectra (transmission geometry) of $Y_{1-x}Er_xAl_3(BO_3)_4$ glassy thin films prepared by PP and SG methods excited at $\lambda = 980$ nm.

The film refractive index is smaller than that of Er-doped crystal [28] (Table 1) due to the glassy nature of the layers that is typically more distorted, and thus less dense, than the crystalline one.

The dependency of film thickness on the Er concentration can be associated to typical changes of small discrepancies on solution viscosity. Indeed, if the viscosity of the initial solution deposited on the substrate is higher than other, the resulting film thickness is higher. But, we can also note that the samples with $x = 0.05$ and 0.10 Er concentrations exhibit higher thicknesses and lower refractive indices. Thus, these higher thicknesses can be associated to a not well-densified deposit having low refractive index.

The films exhibit strong PL emission around 1530 nm. The PP waveguides have higher PL efficiencies and lower propagation losses than the SG ones. This is in good agreement with the coupling efficiencies observed for the PP thin films [24]. For both film types, the $x = 0.10$ composition showing the highest PL intensity. This observation is correlated to the lifetime quenching concentration which is in between $x = 0.1$ and $x = 0.3$ for both film types. This high quenching concentration is also observed in erbium-doped c-YAB crystals. However, the related low emission lifetime in the order of 600 μs was also observed also in our a-YAB films. These two features are typical for borate based host matrices. In fact the main result of our work is that we could reproduce the main spectroscopic properties of doped c-YAB in our a-YAB thin films.

5. Conclusions

We have studied the optical transmission and PL emission of erbium-doped a-YAB planar waveguides prepared by the PP and SG

chemical routes. The film thicknesses and refractive indices were determined by two approaches: the envelope method from the optical transmission spectra and the *m*-lines spectroscopy in the visible and near infrared region. The very good agreement on film thicknesses for the two methods, confirmed also by the HR-SEM results, demonstrated the validity of the envelope calculations. On the other hand, the refractive indices calculated for $\lambda = 633$ nm are similar from both envelope and m-lines calculations: $n = 1.6207$ and 1.6862 from optical transmission spectra, $n = 1.61$ and 1.6735 from *m*-lines spectroscopy for PP and SG thin films, respectively. The erbium concentration, x, affects the refractive index with minimum values around $x = 0.05$–0.10 that are certainly due to differences of film densifications associated to $T_{g(x)}$ variations. Finally, the PP films, especially with the $x = 0.10$ composition, seems to be the most promising waveguide due to the lowest propagation loss value (0.52 ± 0.14 dB/cm at $\lambda = 633$ nm), which is associated to high photoluminescence emission around 1530 nm.

Acknowledgments

The support of FAPESP and CNPq (Brazilian agencies), and CAPES-COFECUB Brazil–France cooperation program is gratefully acknowledged.

References

[1] W.H. Wong, K.S. Chan, E.Y.B. Pun, Appl. Phys. Lett. 87 (2005) 11103.
[2] Y.B. Choi, S.H. Cho, D.C. Moon, Opt. Lett. 25 (2000) 263.
[3] S. Taccheo, G. Della Valle, R. Osellame, G. Cerullo, N. Chiodo, P. Laporta, O. Svelto, A. Killi, U. Morgner, M. Lederer, D. Kopf, Opt. Lett. 29 (2004) 2626.
[4] N.A. Stathopoulos, S.P. Savaidis, Opt. Commun. 281 (2008) 80.
[5] Z. Xiao, F. Xu, T. Zhang, G. Cheng, L. Gu, J. Phys.: Condens. Matter 14 (2002) 11315.
[6] N.A. Tolstik, V.E. Kisel, N.V. Kuleshov, V.V. Maltsev, N.I. Leonyuk, Appl. Phys. B 97 (2009) 357.
[7] Y.P. Rudnitskii, L.V. Shachkin, I.D. Zalevskii, Quantum Electron. 32 (2002) 197.
[8] S. Jiang, M. Myers, N. Peyghambarian, J. Non-Cryst. Solids 239 (1998) 143.
[9] F.F. Sene, J.R. Martinelli, L. Gomes, J. Non-Cryst. Solids 348 (2004) 271.
[10] R.R. Gonçalves, Y. Messaddeq, A. Chiasera, Y. Jestin, M. Ferrari, S.J.L. Ribeiro, Thin Solid Films 516 (2008) 3094.
[11] W.X. Que, X. Hu, J. Zhou, Thin Solid Films 484 (2005) 278.
[12] P.G. Kik, A. Polman, MRS Bull. 23 (1998) 48.
[13] J. Fick, E.J. Knystautas, A. Villeneuve, F. Schittekatte, S. Roorda, K.A. Richardson, J. Non-Cryst. Solids 271 (2000) 200.
[14] S.Y. Chen, C.C. Ting, C.H. Li, J. Mater. Chem. 12 (2002) 1118.
[15] J. Qiu, A. Makishima, J. Nanosci. Nanotechnol. 5 (2005) 1541.
[16] W. You, Y. Huang, Y. Chen, Y. Lin, Z. Luo, Opt. Commun. 281 (2008) 4936.
[17] W. You, Y. Huang, Y. Chen, Y. Lin, Z. Luo, Physica B 405 (2010) 34.
[18] A. Szysiak, L. Lipinska, W. Ryba-Romanowski, P. Solarz, R. Diduszko, A. Pajaczkowska, Mater. Res. Bull. 44 (2009) 2228.
[19] J. Liao, Y. Lin, Y. Chen, Z. Luo, Y. Huang, J. Crystal Growth 267 (2004) 134.
[20] L.J.Q. Maia, A. Ibanez, J. Fick, N. Sanz, A.C. Hernandes, V.R. Mastelaro, J. Nanosci. Nanotechnol. 7 (2007) 3629.
[21] L.J.Q. Maia, V.R. Mastelaro, S. Pairis, A.C. Hernandes, A. Ibanez, J. Solid State Chem. 180 (2007) 611.
[22] L.J.Q. Maia, A. Ibanez, N. Sanz, V.R. Mastelaro, A.C. Hernandes, J. Nanoparticle Res. 10 (2008) 1251.
[23] L.J.Q. Maia, C.R. Ferrari, V.R. Mastelaro, A.C. Hernandes, A. Ibanez, Solid State Sci. 10 (2008) 1835.
[24] L.J.Q. Maia, V.R. Mastelaro, A.C. Hernandes, J. Fick, A. Ibanez, Thin Solid Films 517 (2009) 6584.
[25] J.C. Manifacier, J. Gasiot, J.P. Fillard, J. Phys. E 9 (1976) 1002.
[26] C.H. Peng, S.B. Desu, J. Am. Ceram. Soc. 77 (1994) 929.
[27] H. Liu, X. Chen, L.X. Huang, X. Xu, G. Zhang, N. Ye, Mater. Res. Innov. 15 (2011) 140.
[28] R. Martínez Vázquez, R. Osellame, M. Marangoni, R. Ramponi, E. Diéguez, Opt. Mater. 26 (2004) 231.
[29] Q. Xiang, Y. Zhou, B.S. Ooi, Y.L. Lam, Y.C. Chan, C.H. Kam, Thin Solid Films 370 (2000) 243.
[30] G. Nunzi Conti, S. Berneschi, M. Brenci, S. Pelli, S. Sebastiani, G.C. Righni, C. Tosello, A. Chiasera, M. Ferrari, Appl. Phys. Lett. 89 (2006) 121102.
[31] W.A. Pisarski, J. Mater. Sci.: Mater. Electron. 17 (2006) 245.
[32] L.J.Q. Maia, J. Fick, C. Bouchard, V.R. Mastelaro, A.C. Hernandes, A. Ibanez, Opt. Mater. 32 (2010) 484.